Gaussian Process Tomography of carbon radiation in the transition to detached plasmas in the Wendelstein 7-X stellarator

M. Krychowiak[1], R. König[1], F. Henke[1], T. Barbui[2], E. Flom[3], S. Kwak[1], J. Svensson[1], D. Gradic[1], Y. Feng[1], Y. Gao[1], M. Jakubowski[1], M. Otte[1], F. Reimold[1], O. Schmitz[3], V. Winters[1], D. Zhang[1], T. Sunn Pedersen[1] and the W7-X Team*

[1]*Max-Planck-Institute for Plasma Physics, Greifswald, Germany*

[2]*Princeton Plasma Physics Laboratory, Princeton, New Jersey 08543, USA*

[3]*Univ. of Wisconsin, Dept. of Engineering Physics, Madison, WI 53706, USA*

T. Klinger et al 2019 Nucl. Fusion 59 112004

During the most recent experimental campaign OP1.2b of the optimised stellarator Wendelstein 7-X (W7-X) full thermal detachment of the plasma from the divertor plates was observed [1]. A high performance plasma in the standard magnetic configuration (SDC) heated with ~6 MW of electron cyclotron resonance heating was well stabilised in detached conditions over 28 sec. using feedback controlled H_2 fuelling with the line-integrated electron density ($\int n_e dl$ ~1.1×10^{20} m^{-2} in this discharge) as control parameter [2]. At these high densities, the thermal detachment was accompanied by high recycling of neutrals at the divertor targets and hence significant neutral pressures in the subdivertor volume of up to 2×10^{-3} mbar (in the high-iota configuration), which allowed balancing the fuelled particles by gas pumping through the divertors in some discharges. The optimum detachment working point with respect to particle exhaust was found at the radiation fraction of ~80% in the SDC, as also predicted by EMC3-EIRENE simulations [1] [3]. In the transition to the detachment the divertor plasma cools down such that the impurity radiation moves from the target plates towards the separatrix. The dynamics of carbon line emission was experimentally investigated using comprehensive spectroscopic observation systems at two divertors [4]. At each divertor 27 lines of sight (LOS) were directed parallel to the horizontal target in addition to 27 perpendicular LOS (Figure 1). Several spectrometers with CCD cameras were utilised with a wide range of spectral resolution of 0.003-1 nm for various applications. For tomographic reconstruction of carbon radiation at the divertor spectrometers with focal lengths of 160 were used. The two fans of LOS are spanning two surfaces at an angle of 25° and cross each other close to the horizontal divertor. We simplify the tomography model by an assumption of both fans lying on the same surface (of the horizontal LOS). This should not have a significant effect on the results since the toroidal distance of the real and assumed emission points is small (< 8 cm) and the real emission can be assumed to not change significantly along the short (toroidal) distance.

The inversion is done in the Bayesian modelling framework Minerva [5] applying Gaussian Process Tomography (GPT) [6]. Plasma emission at the divertor is modelled on a 2D grid (with ~30×50 points along the R and Z coordinate) indicated with the orange box in Figure 1. The prior distribution for the 2D emission is set to be a Gaussian process prior with a squared

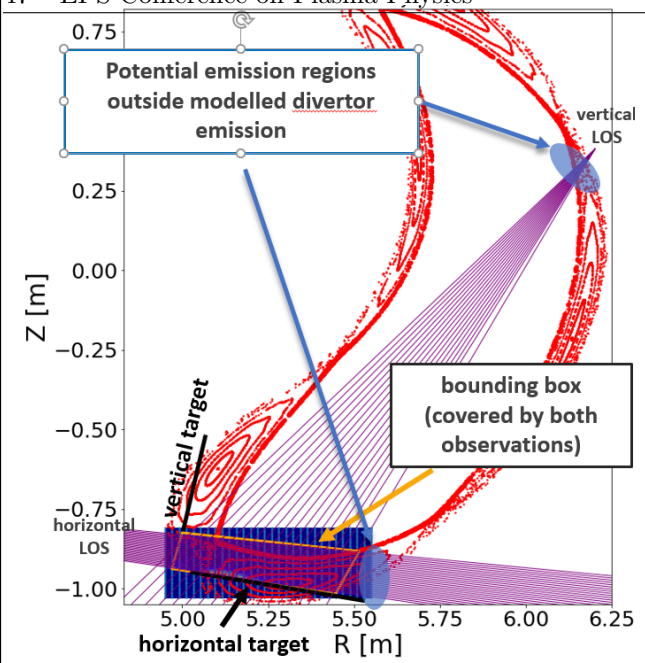

Figure 1 Poincare plot of the separatrix and magnetic islands as well as the divertor target plates in the plane of the spectroscopic observation with the fans of horizontal and vertical LOS.

exponential covariance function. This GP prior is non-parametric with the only assumption on hyperparameters that describe the correlation length scales in the R and Z direction constraining the emission profile smoothness along these two directions. The GP based tomography model is linear and the posterior distribution can be in principle calculated analytically. However, to avoid negative emissions, the GP prior distribution needs truncation to force positive values and therefore requires a sampling from the posterior distribution which takes ~1 min for each time slice. The Bayesian Occam's razor principle is used in a first step to find optimum length scales, which keep the model complexity at a minimum level necessary to predict the measurements within their error bars. The typical optimum length scales found in the analysed experiments lie at 1-2.5 cm in the Z direction and 4-13 cm in the R direction. Since modelling the emission only within the orange bounding box does not account for possible edge emission outside of the box at the two positions indicated in Figure 1 with blue ellipses, we add 1D profiles (as function of LOS number, also modelled with a Gaussian Process) of the so-called horizontal and vertical background emission to the signal prediction of the horizontal and vertical LOS. Larger background emission is expected in the vertical LOS signals since the viewing chords cross also the opposite plasma edge close to the observation port. Uncertainties and correlations of the inferred 2D emission profiles (within the

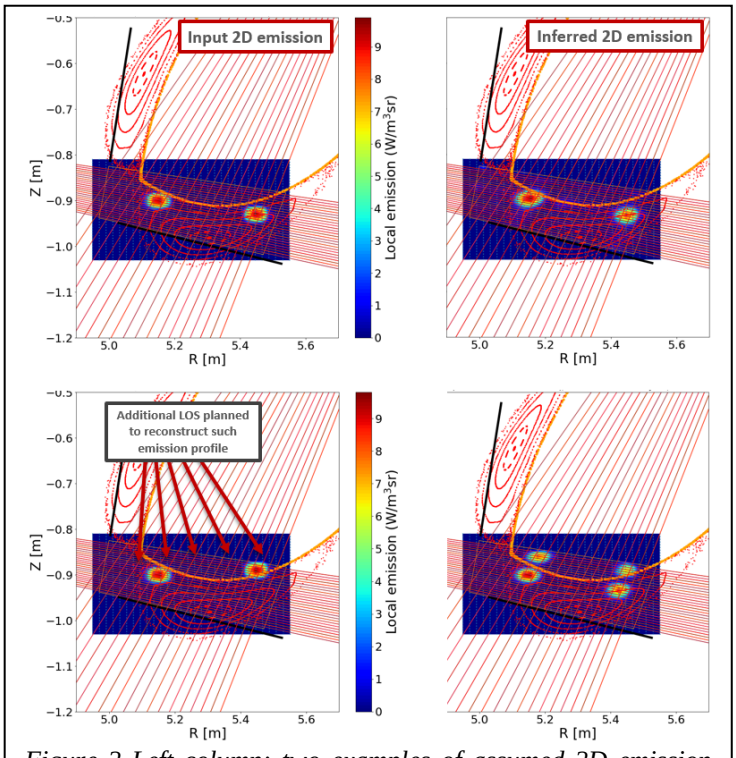

Figure 2 Left column: two examples of assumed 2D emission used to create synthetic observations. Right column: reconstructed emission.

bounding box) and of the backgrounds are provided by final samples from the posterior distribution.

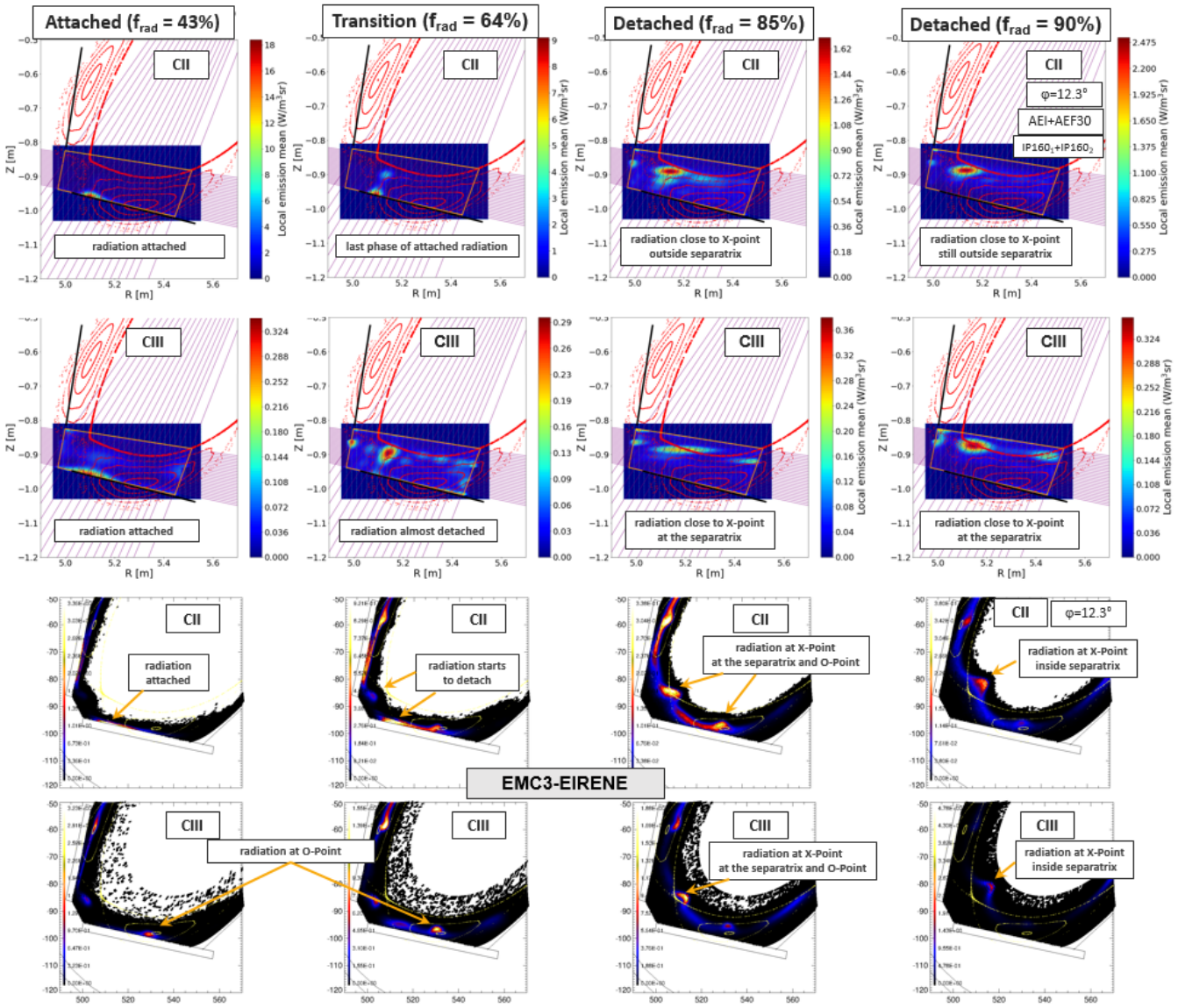

Figure 3 Rows 1-2: reconstructed CII (712 nm) and CIII (674 nm) emission profiles at four time points (5.0 s., 5.43 s., 5.58 s., 5.72 s.) of the discharge 20181010.027 in the transition from attached to detached plasma. In columns 1-4 the results are shown for increasing plasma density and by this increasing fraction of radiated power (f_{rad}). Rows 3-4: total CII and CIII radiation modelled with EMC3-EIRENE code for similar plasma parameters and same f_{rad} values.

Inferring the 2D emission and the two background emission profiles poses an under-determined problem and needs further constraints to reduce the space of allowed solutions. We limit the length scale of the background profiles to some minimum value (e.g. 10 in units of LOS number) since, based on EMC3-EIRENE simulations, we do not expect very small scales in the background emission structures. Another limitation is imposed by the fact of observing the plasma from only two directions. In order to check the sanity of the tomography model and its limitations, reconstruction of synthetic (noised) data was performed. Figure 2 shows two examples of double emission zones assumed to create the synthetic observation: in the first case both zones lie outside of the separatrix (upper row in Figure 2), in the second case one emission zone is assumed to lie inside the separatrix (lower row in Figure 2). While in the first case the input emission profile is well reconstructed, the mean values of the posterior distribution in the

second case show four emission zones. This is plausible since only two observation directions don't provide sufficient information to reconstruct more complex emission profiles. Such cases will require further constraints of the parameter space, e.g. by assuming constant n_e and T_e on flux surfaces inside the separatrix, and are planned in future work.

In the upper two rows of Figure 3 the reconstructed 2D emission (CII and CIII at the wavelengths 712 nm and 674 nm, respectively) at the divertor is shown. Four time points are selected in the discharge 20181010.027 (run in SDC with +2kA of control coil currents) in which $\int n_e dl$ was linearly increased from 0.8 to 1.2×10^{20} m^{-2} accompanied by a non linear monotonic increase of the radiated heating power fraction f_{rad} from 20% to 95%. At f_{rad} of ~55% the convective peak heat loads to the divertor (not shown) start to drop significantly and the transition into detachment sets in. At f_{rad} = 43% CII and CIII radiation is attached to the horizontal target at the place of the strike line (with the maximum convective heat loads) close to the vertical target. In the transition phase, at f_{rad} = 64%, the edge plasma cools down sufficiently for CIII emission to detach and move towards the separatrix while CII emission is still attached. At the next two points in time (f_{rad} = 85% and 90%) also CII radiation is detached, however it stays slightly outside the separatrix, while CIII radiation sits at the separatrix. In EMC3-EIRENE modelling (lower two rows of Figure 3) of a discharge with similar, but not the same parameters (e.g. with control coil currents of 0 kA), we see similar dynamics of the CII emission. In contrast, CIII emission at the two first time points (f_{rad} = 46% and 64%) is concentrated at the O-Points and moves to the X-Point only in detachment. Another difference is observed in the radial position of the radiation in detachment: while the modelling predicts both CII and CIII emission inside the separatrix, the emission in experiment is seen slightly outside (CII) or at (CIII) the separatrix. These differences can result from some physics phenomena missing in the modelling (e.g. particle drifts) on the one side and from experimental uncertainties and assumptions made in the ill-posed tomography model on the other side. The uncertainties of the reconstructed emission will be improved in the next experiments (e.g. by adding LOS at a third observation port, see Figure 1) with the aim to support further refinements of the EMC3-EIRENE physics model of the divertor plasmas.

REFERENCES

[1] Schmitz, O. et al., *Nucl. Fusion,* p. 016026 (27pp), 61 (2021) .
[2] Jakubowski, M. et al., *Nucl. Fusion,* 2021 (submitted).
[3] Feng Y. et al., *Nucl. Fusion,* 2021 (accepted for publication).
[4] Barbui T. et al., *JINST*, p. 14 C07014, 2019.
[5] Svensson J. and Werner A., *International Symposium on Intelligent Signal Processing-WISP (IEEE),* 2007 Vol. 955.
[6] J. Svensson, "Nonparametric tomography using Gaussian processes," *JET Internal Report No. EFDA-JET-PR(11) 24,* 2011.